Coherent Distributed Bistatic Radar Using Wireless Frequency Syntonization and Internode Ranging

Anton Schlegel, *Graduate Student Member, IEEE*, Jason M. Merlo, *Graduate Student Member, IEEE*, and Jeffrey A. Nanzer, *Senior Member, IEEE*

***Abstract*— We present a distributed microwave radar system operating at 4.8 GHz that uses wireless frequency transfer and internode ranging. We implement wireless frequency alignment (syntonization) using a sparse two-tone signal transmitted from the primary node and a self-mixing receiver on the secondary node. The primary node acts as a distributed radar transmitter, sending a linear frequency-modulated (LFM) waveform downrange, toward the target. There is also a repeater that retransmits an LFM from the secondary node that is used to estimate the separation of the node to correct for the phase rotation of the frequency signal due to propagation. The secondary node also locks its oscillator to the primary node and captures the signal reflected from the scene. We demonstrate the ability of the fully wireless distributed radar system to perform bistatic ranging in an outdoor environment at 4.8 GHz using software-defined radios (SDRs). Measurements to a wall yielded a maximum standard deviation of 1.7 cm and a maximum bias of 14.9 cm.**

***Index Terms*— Coherent distributed systems, distributed radar, distributed wireless systems, wireless syntonization.**

I. Introduction

BISTATIC radar systems, in which the transmitter and the receiver are sufficiently separated that the reflected radar signal travels over a different path than the transmitted signal, are useful in numerous sensing applications due to their unique characteristics compared to monostatic radar systems [1], [2]. In applications such as radar measurements of the Earth [3], [4], specularity causes the obliquely transmitted signals to scatter largely in directions away from the transmitter; these reflections can be captured in a bistatic receiver to measure, for example, surface tomography [5], [6]. Signals of opportunity are often used in bistatic radar, such as reflected GNSS signals or other noncooperative signals [7], [8], [9], [10], [11].

A significant challenge to implementing a cooperative bistatic radar system is in aligning the frequencies (*syntonizing*) of the local oscillators on the platforms and in estimating the relative separation between the nodes. While synchronization of the timing of distributed systems has been studied using various techniques [12], distributed bistatic radar sensing relies on accurate syntonization, which does not necessarily require high-accuracy time synchronization. If the oscillators are syntonized and the relative separation between the nodes is accurately estimated, the bistatic range can be determined by estimating the delay difference between the direct path radar signal transmitted between the two nodes and the bounce path reflected off the scene. The delay estimation and frequency syntonization requirements depend on several factors including platform motion and waveform bandwidth [13]; several methods have been proposed to compensate for the delay and frequency requirements of the two platforms. While syntonization may be implemented using high-accuracy synchronization (e.g., [14], [15]), direct syntonization can be implemented with less processing overhead using adjunct circuitry [16], [17].

In this letter, we present a novel distributed bistatic radar system based on wireless coordination at the wavelength level. The radar consists of two software-defined radio (SDR)-based nodes that utilize wireless syntonization combined with internode range estimation to align the phases of the systems. The transmitting node emits a linear frequency-modulated (LFM) waveform directly to the receiving node and also downrange. The receiving node captures the two waveforms and estimates the bistatic elliptical range from the difference between the arrival times of the two waveforms. The receiving node also estimates the internode range that is used in the bistatic range estimation and also corrects for dynamic syntonization phase changes due to platform motion. Although prior works on distributed wireless systems have demonstrated coordinated transmission, to our knowledge, this work is the first to demonstrate coherent distributed sensing using real-time coordination and processing on moving platforms that does not require postprocessing.

II. Distributed Bistatic Radar System Design

The distributed radar system measures the bistatic isorange ellipse $R = R_i - R_d$, where R_i is the indirect (downrange) distance estimate and R_d is the direct (internode) range estimate. To operate without significant postprocessing, both R_i and R_d must be estimated in real time, necessitating coherent distributed signal processing. We support this via wirelessly locking the oscillators and by directly measuring R_d. The

Manuscript received 2 March 2023; revised 18 April 2023; accepted 31 May 2023. Date of publication 17 July 2023; date of current version 6 September 2023. This work was supported in part by the Air Force Research Laboratory under Contract FA8650-14-D-1725, in part by the Office of Naval Research under Grant N00014-20-1-2389, and in part by the National Science Foundation under Grant 1751655. *(Corresponding author: Jeffrey A. Nanzer.)*

The authors are with the Department of Electrical and Computer Engineering, Michigan State University, East Lansing, MI 48824 USA (e-mail: schleg19@msu.edu; merlojas@msu.edu; nanzer@msu.edu).

Color versions of one or more figures in this letter are available at https://doi.org/10.1109/LMWT.2023.3283918.

Digital Object Identifier 10.1109/LMWT.2023.3283918

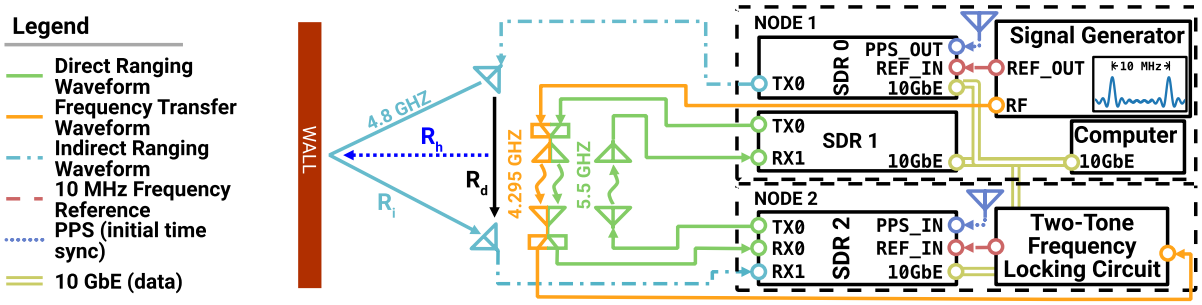

Fig. 1. Block diagram of the SDR-based distributed bistatic radar system. Node 1 transmits the bistatic radar waveform downrange and transmits a frequency reference directly to Node 2. Node 2 simultaneously transmits an internode-ranging waveform to estimate the direct distance between the nodes. Node 2 receives the scattered bistatic radar signal and the wireless frequency reference and uses the direct range estimate to compute the bistatic range.

wireless frequency reference undergoes a phase rotation as the platforms move relative to one another, causing errors in the indirect range estimate if left uncorrected. The direct range R_d is thus also used to correct this phase error to yield accurate indirect range estimates. The direct range R_d is estimated by transmitting a waveform from the radar receiver node to the radar transmitter node, which then retransmits the signal back to the radar receiver node. This range must be calibrated to correct for system latencies and is given by $R_d = R_{\text{est}}/2 + R_{\text{cal}}$ where R_{est} is the total estimated range and R_{cal} is the experimentally determined calibration. The direct range estimate R_d is obtained via a coherent process since the same waveform is repeated back to the radar receiver node; while a phase offset may be imparted, the frequency is the same. Accurate estimation of the indirect range R_i is more challenging since the transmitter and the receiver are separate systems with separate local oscillators. Wireless syntonization is used to lock the oscillators; however, as the nodes move the delay associated with the propagation of the frequency reference changes, imparting phase changes that manifest as range estimation errors. This phase delay, being commensurate with the internode distance, is calculated from the direct range R_d and used to correct for the additional phase offset during the measurement process, enabling a fully wireless coherent distributed bistatic radar measurement. While the measurement process, in general, yields the bistatic isorange ellipse, if the target is broadside to the baseline of the array, the distance to the target can be estimated by $R_h = ((R_i/2)^2 - (R_d/2)^2)^{1/2}$.

The system consists of two SDR-based nodes as shown in Fig. 1. The transmitter (the primary node, also referred to as Node 1) has two Ettus USRP X310 SDRs and a Keysight E8267D signal generator used to generate the frequency reference. The frequency reference is transmitted continuously between the two nodes to lock the oscillators. The system is initially synchronized using an external pulse-per-second signal, after which the nodes remain synchronized as long as the wireless frequency transfer link is operational. At a set periodicity, Node 1 transmits an LFM waveform in the downrange direction, which is captured by Node 2 to estimate the indirect range R_i. Simultaneously, Node 2 transmits an LFM toward Node 1, which captures and retransmits the signal using an SDR-based repeater; this signal is then received by Node 2 to estimate the direct range R_d.

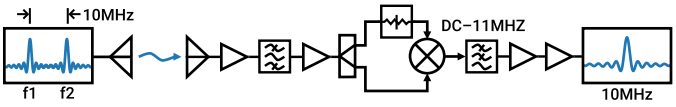

Fig. 2. Schematic of the two-tone wireless frequency locking circuit [18]. The primary node transmits a two-tone signal, the frequency separation of which is equal to the desired reference frequency. The circuit mixes the received signal with a copy of the same signal, demodulating the frequency reference. Residual harmonics are filtered, after which the signal is input to the PLL on the secondary node.

Wireless frequency locking is supported by continuously transmitting a two-tone signal from the signal generator, the frequency separation of which is equal to the desired reference frequency [18], which in this work is 10 MHz. This continuous-wave two-tone waveform is captured at the radar receiver node and is input into a self-mixing circuit as shown in Fig. 2. The self-mixing circuit includes a bandpass filter to mitigate any interfering signals as well as initial amplification at the carrier frequency. The bandpass-filtered waveform is split and input to the RF and LO ports of a mixer (the RF signal is attenuated to avoid compression). This demodulates the frequency reference, which is the beat frequency between the two tones, to baseband where it can be input to the phase-locked loop (PLL) of the SDR on the secondary node. The output signal is low-pass filtered to mitigate any residual harmonic signals that manifest from the self-mixing process and then amplified and input to the PLL, locking the frequencies of the two nodes.

III. Experimental Validation and Results

We conducted experiments in an outdoor environment as shown in Fig. 3. Each node was implemented on a mobile cart and was initially placed 2 m apart, while the indirect ranging antennas were directed toward a flat wall that was a distance of 3 m from the system (longer ranges could be supported with transmit amplification). The primary node was kept stationary, and the secondary node was moved linearly in a path parallel to the wall, thus the distances between the nodes and the wall were approximately equal. The direct and indirect waveforms were both 10-μs LFM waveforms with 100-MHz bandwidth, transmitted every 1 s. The transmitted and received waveforms were sampled at 200 MSps. Matched filtering was performed on both received waveforms to estimate the delay and thus the range. The frequency-locking waveform was a continuous

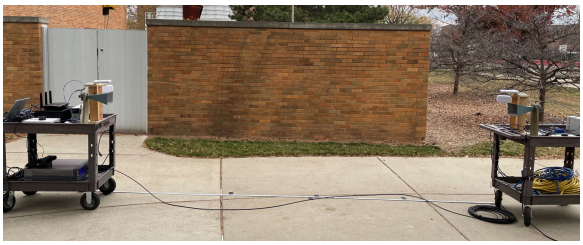

Fig. 3. Distributed bistatic radar experimental setup.

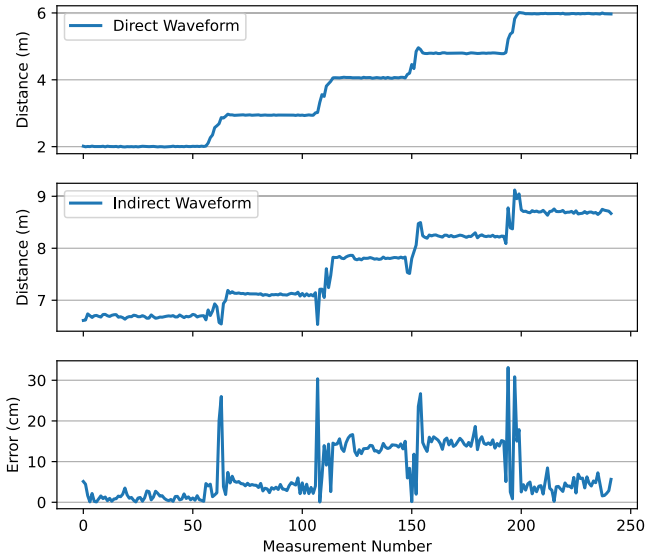

Fig. 4. (Top) Measurements of the direct range. (Center) Measurements of the indirect range, showing slightly increased variance due to the wireless frequency transfer. (Bottom) Absolute measurement error of bistatic distance to the wall. Large spikes in the measurements are due to relative Doppler as the nodes are moved; this may be corrected with additional signal processing.

waveform with a carrier frequency of 4.295 GHz and an upper sideband of 4.305 GHz. The indirect radar waveform was implemented at a 4.8-GHz carrier frequency, while the direct ranging waveform was implemented at a 5.5-GHz carrier frequency. An initial calibration was conducted to account for phase delays due to the cables and processing time (latency) in the SDRs, which was conducted by pointing the bistatic (indirect) antennas toward each other, thus any phase delays in the indirect ranging path were also corrected. The processing time was not optimized; on the host computer, it was ∼2 ms; offline processing to generate the range profile was ∼50 ms.

The primary node was kept stationary, while the secondary node was moved in 1-m steps. At each step, the secondary node paused for 30 s before moving to the next step. The distance from the nodes to the wall was then estimated from the bistatic range R, assuming that the angles of the paths from the transmitter and the receiver to the wall were identical and thus that the path lengths were identical. It was assumed that the paths from both the transmitter and the receiver to the scattering point were identical. The range was estimated for both the direct and indirect ranges. A laser range finder was used to measure the distance to the wall at each step as a control measurement. Quadratic least-squares interpolation was used to refine the range measurement [19, Ch. 7.2]. The direct range estimation—distance between the nodes—is shown in Fig. 4(Top). The movement of the cart in 1-m steps

TABLE I
MEASUREMENT SUMMARY

Step	R_d (m)	R_i (m)	R_h (m)	σ (cm)	Bias (cm)
1	2.00	6.87	3.19	1.2	0.9
2	2.94	7.12	3.24	0.7	–3.8
3	4.06	7.81	3.34	1.2	–13.6
4	4.79	8.24	3.35	1.2	–14.9
5	5.97	8.70	3.16	1.7	4.0

can be seen. The indirect range estimation—range off the wall—is shown in Fig. 4(Center). Since the direct waveform is estimated by transmitting and receiving from the same system (SDR2 in Fig. 1), the estimation error is lower than that of the indirect range; in the latter case, the error is compounded by the effect of wirelessly locking the oscillators on the transmitter and the receiver, while the direct ranging system is self-coherent. The error in measuring the distance to the wall is shown in Fig. 4(Bottom). Table I shows the calculated internode distances, the standard deviation of the wall range at each internode distance, and the bias between the calculated and measured distances. At each range step, 25 measurements were used to calculate the data in the table. The standard deviation of the range estimate at each range step is no more than 1.7 cm, and the bias at each range step is no more than 4.65% of the measured range to the wall. There exist larger transient errors in the range measurement that correspond to times when the nodes were moving; these were due to relative Doppler manifesting on the radar signals. This error could be corrected via Doppler estimation. The larger bias at some distances is likely due to errors manifesting from the assumption that the ranges between the transmitter and the receiver to the wall are identical, as well as multipath impacts on the wireless frequency transfer link.

IV. CONCLUSION

We demonstrated the feasibility of distributed bistatic ranging measurements using wireless frequency transfer and internode ranging achieving precision of <2 cm and bias of <15 cm. By wirelessly transferring a frequency reference and estimating the change in the internode range, accurate estimates of the bistatic range can be computed in real time without the need for postprocessing. These results provide a framework for future distributed microwave wireless sensing systems on moving platforms. While this work demonstrated a two-node bistatic distributed radar system, the approach could be directly extended to multistatic systems using scalable relative position estimation and syntonization approaches such as those demonstrated in [20] and [21] and could be implemented in dynamic scenarios using adaptive coordination approaches [16].

ACKNOWLEDGMENT

Distribution Statement A: Approved for Public Release. Distribution is Unlimited. APRS-RYM-2023-06-00002.

REFERENCES

[1] M. I. Skolnik, "An analysis of bistatic radar," *IRE Trans. Aerosp. Navigational Electron.*, vol. 8, no. 1, pp. 19–27, 1961.
[2] H. D. Griffiths, "From a different perspective: Principles, practice and potential of bistatic radar," in *Proc. Int. Conf. Radar*, 2003, pp. 1–7.

[3] J. Kubanek, M. P. Poland, and J. Biggs, "Applications of bistatic radar to volcano topography—A review of ten years of TanDEM-X," *IEEE J. Sel. Topics Appl. Earth Observ. Remote Sens.*, vol. 14, pp. 3282–3302, 2021.

[4] N. L. Bienert et al., "Post-processing synchronized bistatic radar for long offset glacier sounding," *IEEE Trans. Geosci. Remote Sens.*, vol. 60, 2022, Art. no. 1001917.

[5] G. Krieger et al., "TanDEM-X: A satellite formation for high-resolution SAR interferometry," *IEEE Trans. Geosci. Remote Sens.*, vol. 45, no. 11, pp. 3317–3341, Nov. 2007.

[6] S. Duque, P. Lopez-Dekker, and J. J. Mallorqui, "Single-pass bistatic SAR interferometry using fixed-receiver configurations: Theory and experimental validation," *IEEE Trans. Geosci. Remote Sens.*, vol. 48, no. 6, pp. 2740–2749, Jun. 2010.

[7] J. S. Malik and U. I. Bhatti, "Remote sensing of ocean, ice and land surfaces using bistatically reflected GNSS signals from low Earth orbit," in *Proc. 4th Int. Conf. Aerosp. Sci. Eng. (ICASE)*, Sep. 2015, pp. 1–6.

[8] J. Song, W. Xiong, X. Chen, and Y. Lu, "Experimental study of maritime moving target detection using hitchhiking bistatic radar," *Remote Sens.*, vol. 14, no. 15, p. 3611, Jul. 2022. [Online]. Available: https://www.mdpi.com/2072-4292/14/15/3611

[9] A. R. Persico, P. Kirkland, C. Clemente, J. J. Soraghan, and M. Vasile, "CubeSat-based passive bistatic radar for space situational awareness: A feasibility study," *IEEE Trans. Aerosp. Electron. Syst.*, vol. 55, no. 1, pp. 476–485, Feb. 2019.

[10] J. Brown, K. Woodbridge, H. Griffiths, A. Stove, and S. Watts, "Passive bistatic radar experiments from an airborne platform," *IEEE Aerosp. Electron. Syst. Mag.*, vol. 27, no. 11, pp. 50–55, Nov. 2012.

[11] M. Plotka, M. Malanowski, P. Samczynski, K. Kulpa, and K. Abratkiewicz, "Passive bistatic radar based on VHF DVB-T signal," in *Proc. IEEE Int. Radar Conf. (RADAR)*, Apr. 2020, pp. 596–600.

[12] A. K. Karthik and R. S. Blum, "Recent advances in clock synchronization for packet-switched networks," *Found. Trends® Signal Process.*, vol. 13, no. 4, pp. 360–443, 2020.

[13] M. Weiss, "Synchronisation of bistatic radar systems," in *Proc. IEEE Int. Geosci. Remote Sens. Symp.*, May 2004, pp. 1750–1753.

[14] S. Prager, M. S. Haynes, and M. Moghaddam, "Wireless subnanosecond RF synchronization for distributed ultrawideband software-defined radar networks," *IEEE Trans. Microw. Theory Techn.*, vol. 68, no. 11, pp. 4787–4804, Nov. 2020.

[15] J. M. Merlo, S. R. Mghabghab, and J. A. Nanzer, "Wireless picosecond time synchronization for distributed antenna arrays," *IEEE Trans. Microw. Theory Techn.*, vol. 71, no. 4, pp. 1720–1731, Apr. 2023.

[16] S. R. Mghabghab, A. Schlegel, and J. A. Nanzer, "Adaptive distributed transceiver synchronization over a 90 m microwave wireless link," *IEEE Trans. Antennas Propag.*, vol. 70, no. 5, pp. 3688–3699, May 2022.

[17] S. R. Mghabghab and J. A. Nanzer, "Open-loop distributed beamforming using wireless frequency synchronization," *IEEE Trans. Microw. Theory Techn.*, vol. 69, no. 1, pp. 896–905, Jan. 2021.

[18] S. Mghabghab, H. Ouassal, and J. A. Nanzer, "Wireless frequency synchronization for coherent distributed antenna arrays," in *Proc. IEEE Int. Symp. Antennas Propag. USNC-URSI Radio Sci. Meeting*, Jul. 2019, pp. 1575–1576.

[19] M. A. Richards, *Fundamentals of Radar Signal Processing*. New York, NY, USA: McGraw-Hill, 2014.

[20] S. M. Ellison and J. A. Nanzer, "High-accuracy multinode ranging for coherent distributed antenna arrays," *IEEE Trans. Aerosp. Electron. Syst.*, vol. 56, no. 5, pp. 4056–4066, Oct. 2020.

[21] H. Ouassal, M. Yan, and J. A. Nanzer, "Decentralized frequency alignment for collaborative beamforming in distributed phased arrays," *IEEE Trans. Wireless Commun.*, vol. 20, no. 10, pp. 6269–6281, Oct. 2021.